Journal of Physics: Conference Series **713** (2016) 012006 doi:10.1088/1742-6596/713/1/012006

In-situ formation of solidified hydrogen thin-membrane targets using a pulse tube cryocooler

S Astbury[1], S Bedacht[3], P Brummitt[1], D Carroll[1], R Clarke[1], S Crisp[1], C Hernandez-Gomez[1], P Holligan[1], S Hook[1], J S Merchan[1], D Neely[1,2], A Ortner[3], D Rathbone[1], P Rice[1], G Schaumann[3], G Scott[1], C Spindloe[1], S Spurdle[1], A Tebartz[3], S Tomlinson[1], F Wagner[3], M Borghesi[4], M Roth[3] and M K Tolley[1]

[1]Central Laser Facility, STFC, Rutherford Appleton Laboratory, Harwell Oxford, Didcot, Chilton, Oxon, OX110QX, UK

[2]Department of Physics, SUPA, University of Strathclyde, Glasgow G4 0NG, UK

[3]Institut für Kernphysik, Technische Universität Darmstadt, Schlossgartenstrasse 9, 64289 Darmstadt, Germany

[4]Queen's University Belfast 2015, University Road Belfast, BT7 1NN, Northern Ireland, UK

E-mail: sam.astbury@stfc.ac.uk

Abstract. An account is given of the Central Laser Facility's work to produce a cryogenic hydrogen targetry system using a pulse tube cryocooler. Due to the increasing demand for low Z thin laser targets, CLF (in collaboration with TUD) have been developing a system which allows the production of solid hydrogen membranes by engineering a design which can achieve this remotely; enabling the gas injection, condensation and solidification of hydrogen without compromising the vacuum of the target chamber. A dynamic sealing mechanism was integrated which allows targets to be grown and then remotely exposed to open vacuum for laser interaction. Further research was conducted on the survivability of the cryogenic targets which concluded that a warm gas effect causes temperature spiking when exposing the solidified hydrogen to the outer vacuum. This effect was shown to be mitigated by improving the pumping capacity of the environment and reducing the minimum temperature obtainable on the target mount. This was achieved by developing a two-stage radiation shield encased with superinsulating blanketing; reducing the base temperature from 14 ± 0.5 K to 7.2 ± 0.2 K about the coldhead as well as improving temperature control stability following the installation of a high-performance temperature controller and sensor apparatus. The system was delivered experimentally and in July 2014 the first laser shots were taken upon hydrogen targets in the Vulcan TAP facility.

1. Introduction

Generating ion beams of the desired energy, flux and quality is critical to the advancement of many novel applications[1] such as laser driven ion oncology, Fast Ignition and in fields such as material science. Hadron therapy for example will require nucleon energies $E_{nucleon}$>200 MeV which to date has not been possible to achieve with the current generation of high power lasers.

Experimental work[2] on relativistically-intense (I >10^{18} W/cm^2) laser systems such as the VULCAN Petawatt laser[3] at the Central Laser Facility (CLF), have facilitated the generation of ion beams of energy 10 MeV > E_{proton} > 75 MeV through the Target Normal Sheath Acceleration[4, 5] (TNSA) method of ion acceleration. TNSA is achieved by irradiating a thin target-foil (on the order of

a few microns in thickness) with an ultra intense laser pulse. Energetic fast electrons (MeV-energy) are generated in the laser focus and they are accelerated through the target and propagate out of the rear side of the foil. This escaping charge results in a separation electric field, of TV/m strength which ionizes and accelerates the surface atoms, resulting in the expanding ions travelling quasi normally away from the rear of the target[6]. Any laser pre-pulse of sufficient intensity to ionize the front target surface before the main pulse of the laser arrives, can generate an expanding plasma[7]. This pre-plasma plays a significant role in the subsequent coupling efficiency[8] of the laser and the generation of hot electrons. However, such a pre-pulse can also launch a shock through the target foil[9], and larger target thicknesses must be employed to mitigate damage to the target's integrity (laser contrast dependent). Utilising thicker targets tends to reduce the energy of the resulting proton beam[10] and the intensity scaling ($E_{proton} \propto I^{0.5}$) for TNSA[4,11] alone is not a sufficient driving mechanism to readily meet the needs of applications requiring >200 MeV/nucleon ions.

Simulation studies[12] have suggested the presence of new ion acceleration mechanisms[13] which can be present when an ultra high-contrast laser pulse interacts with a nanometric thick target. By improving the contrast-ratio of the laser pulse, the prepulse plasma is significantly reduced – maintaining target integrity during the early stages of the interaction and enabling further ion acceleration regimes to be accessed, namely enhanced TNSA, Light Sail and Laser Breakout Afterburner (BOA) mechanism. Enhanced TNSA is caused by an improved transfer of the laser energy to the cold target electrons, more efficiently generating hot electrons. These augment the electric fields present in the sheath and cause the ions to accelerate further - particularly in a nanometric target - in a solitary quasi-monoenergetic packet.[14] The Light sail mode utilises radiation pressure[15] to accelerate the ions and the BOA regime manifests itself when the target becomes relativistically transparent. In the latter case in a thin target the electrons are still interacting with the laser field – the propagation of which 'pushes' the electrons, driving a Buneman-instability (a plasmonic instability resulting from a difference in electron and ion velocity of more than the ion-acoustic speed). This imparts a kinetic energy transfer onto the ions at the rear surface of the target.[16] It has been shown via PIC simulations that BOA can theoretically generate ion beams on the order of hundreds of MeV. Such simulations show that the heaviest species present in the target governs the ion velocity of the interaction; thus a low-Z, high purity target is ideal and therefore there is a significant interest in producing solidified pure hydrogen thin films. This paper highlights the work at the Central Laser Facility towards producing an in-situ solidified hydrogen thin film target production capability.

2. Cryogenic target system development:

2.1. Growth Mechanism:

Simulation[17] suggests that for the BOA regime to be realized in solid hydrogen, due to its low-Z, a target thickness of 1-4 μm is ideal. There are three known successful methods of windowless hydrogen target growth, which are: casting[18], extrusion[19] and condensation, all of which were reviewed for efficacy before the development of the system.

The casting method requires the solidified hydrogen to be grown onto a casting plate substrate and then physically removed from a cooled growth surface. Cooling hydrogen using this method can take a long while and due to the stresses involved on the solidified hydrogen during the separation process, thin targets (< 1 mm) cannot reliably be produced and thus use of a casting plate is not a viable method for thin target production.

The second considered approach is the extrusion method. This requires pressurized hydrogen to be forced out of a vessel which has a negative temperature gradient from the top of the vessel to the 'nozzle' out of which the hydrogen is forced as a continuous solidified ribbon. Such a design would require highly pressurized hydrogen inside a vacuum chamber which may not be suitable due to risk of debris damage. Spatial instability is also an inherent issue in such designs as the hydrogen exits the

nozzle and as spatial tolerance is minimal for the focus of the beam, this method is unsuitable for the application discussed.

After considering the above alternative approaches, the condensation method was decided upon for several reasons: lower hydrogen gas pressures are preferential in the laser interaction chamber, quick target growth after system-cooldown and high spatial stability of the hydrogen target.

Hydrogen growth by condensation involves injecting gaseous hydrogen into a sealed environment, henceforth referred to as the growth chamber, in which is a cold surface. This surface is then cooled below the boiling point of H_2 causing the hydrogen gas to condense and fill a target substrate which is then further cooled below the freezing point (T~13.9 K) to solidify the liquid into a thin H_2-ice layer. However, due to the requirement of having a pure hydrogen target, a windowless substrate-free target was an essential criterion of the system.

2.2. Design Parameters:

The main design parameters of the system involve reaching a sufficiently low temperature using a cryogenic cooling system and control of the environmental conditions in the target growth chamber. Figure 1 shows the phase diagram of hydrogen at low pressures, which illustrates the pressure:temperature relationship of hydrogen and its phase transitions.

In order for successful condensation and freezing of a thin-film of hydrogen, a relatively constant vapour pressure on the order of several hundred mbar must be maintained as well as fine temperature control between 10 – 25 K, with a resolution of ~0.3 K; thus a sensor/heater feedback-loop temperature control system was required. From Figure 1, it can be seen that achieving liquefaction requires a minimum pressure of 70.4mbar to be maintained within the growth environment. As this is surrounded by a high vacuum, a leak-tight seal was mandatory and to this end a pressure sensor/readout was critical.

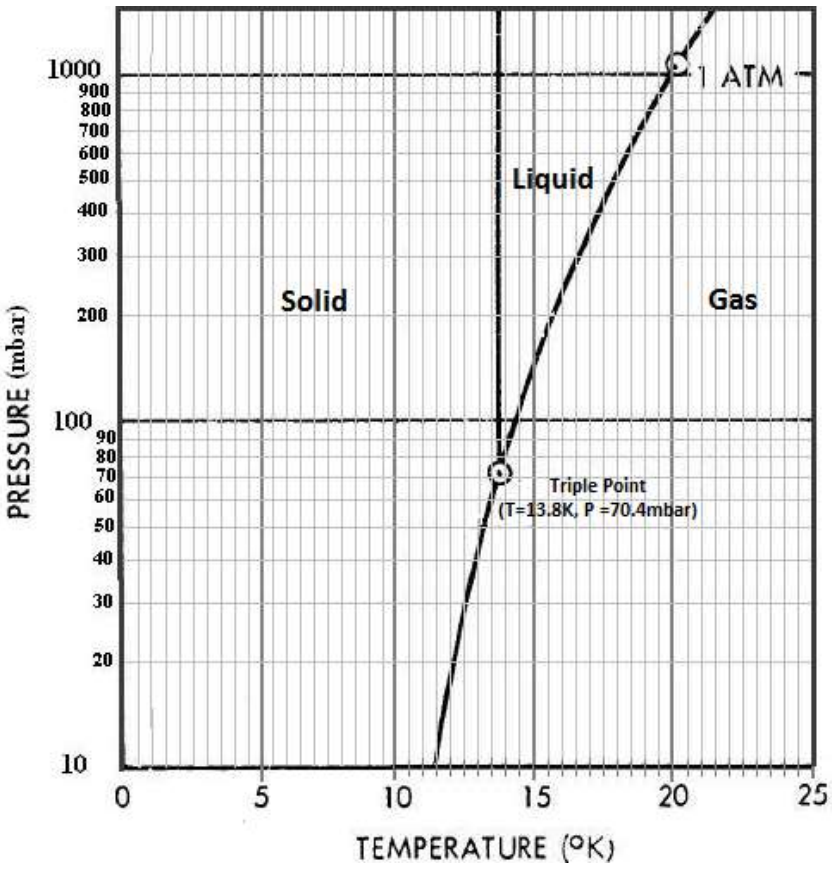

Figure 1. Low pressure phase diagram of hydrogen, showing the solid, liquid and gas regimes and their dependence on pressure and temperature.[20](Reduction from reference)

A hydrogen gas inlet and pump system was necessary to both inject and evacuate the growth chamber during the growth process as well as a sufficiently sized outer vacuum chamber to house the system along with access flanges for a turbo pump, various feedthrough ports and optical diagnostics.

The heater/control system served a secondary purpose to decrease the time taken warming the system back to room temperature before venting the vacuum chamber. This was necessary to prevent condensation/freezing of contaminants onto the apparatus between cooldown/warm-up cycles.

2.3. Conceptual Design:

After consideration and research of the design parameters, a prototype system was designed and installed at CLF[21]. This comprised a Sumitomo RP-082B pulse tube cryocooler which provided 1 W of cooling power at 4.2 K via helium gas compression refrigeration. Such a system does not require cryogenic liquids for cooling, negating the impracticality and cost of cooling via liquid helium.

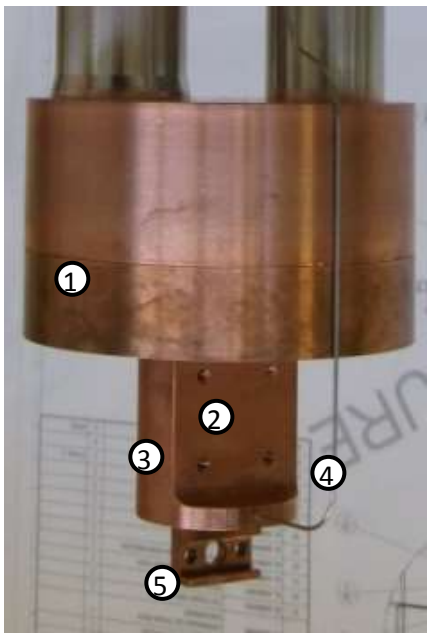

Figure 2. Cryocooler copper coldhead and target mount adapter showing the relevant components of the coldhead.

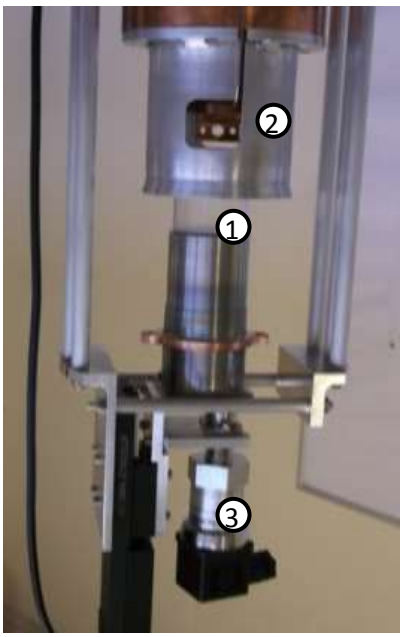

Figure 3. Lower section of the assembly showing the target mount and growth chamber (1), radiation shielding (2) and pressure transducer (3).

The thermal properties of the system were controlled by two 25 Ω resistor heaters and two platinum RTD temperature sensors (mounted at figure 2, label 2 and figure 2, label 3 respectively). Temperature was regulated in the form of an Omega CYC325 temperature controller. This system received input data from the calibrated temperature sensors and controlled the power to the heaters to maintain a setpoint temperature governed by a PID control feedback loop. The total heater output power for the controller was 27 W (1 x 25 W, 1 x 2 W).

The coldhead of the system (figure 2-1) was machined from copper and was designed to provide a high thermal capacity for the target mount to limit susceptibility to sudden temperature spikes which would quickly evaporate the target due to the volatility of hydrogen.

The hydrogen inlet capillary (figure 2-4) also functions as the evacuation line connected to a roughing pump line. This was designed to precool the gas by passing it through the coldhead before injection into the growth chamber and was manually operated using a series of hand valves.

The growth chamber (figure 3-1) comprises a cylindrical polymethyl methacrylate (PMMA) 'cup' which was bolted to the base of the coldhead. A dual indium ring seal ensured the cup was leak-tight. Pressure inside the growth chamber was measured using a transducer (figure 3-3) which connected to the growth chamber via a stainless steel capillary and displayed a digital pressure readout in real-time.

A 2mm thick aluminium shroud acted as a radiation shield (figure 3-2) to prevent thermal radiation from any external heat loads that could raise the temperature around the target. The copper target mount (figure 2-5) consisted of a copper shaft subtending around 25 mm from the coldhead which a target foil could be mounted upon.

The target foils (figure 4) were necessary to promote condensation and growth of the target over an aperture in its centre. These foils were designed to be easily replaceable after the laser interaction with the hydrogen target which would cause inevitable damage to the foil and were positioned horizontally to provide as much thermal contact to the coldhead as possible. Several designs were machined for future research into manipulating the flow of liquefied hydrogen to saturate the target aperture, however for the scope of this project a circular aperture sufficed.

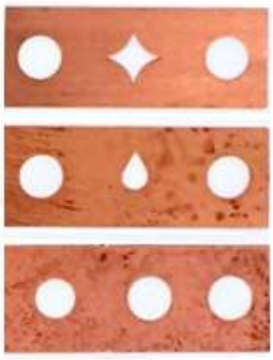

Figure 4. Horizontally mounted copper target foils of various central aperture shapes; spiderweb (top), teardrop (centre) and circular (bottom)

An outer vacuum chamber was constructed to house the system which had a port for a roughing and turbo pump to allow for a vacuum on the order of $1x10^{-5}$ mbar along with feedthrough ports for the components and diagnostics discussed above.

2.4. Base temperature minimisation:

After constructing and assembling a working system within a leak-tight vacuum chamber, research began on achieving a substantially cold base temperature to allow for freezing and survivability of the hydrogen target, i.e. a maximum of 13.9 K (approximate freezing point of hydrogen through the liquid phase at $P > 70.4$ mbar).

By running the pulse tube with the heaters off, the results in Table 1 were gathered which shows the effect on base temperature with and without radiation shielding and superinsulation blanketing. Note for this testing that no hydrogen was injected into the growth chamber which was instead pumped, thus pressure $P \rightarrow 0$ (limited by the impedance of the 1mm capillary from the roughing pump through which it was evacuated). Also worth noting is the fact that the pulse tube cryocooler operates in two stages; 40 W cooling power at 45 K on the first, upper stage and 1 W cooling power at 4.2 K on the second, lower stage.

Shielding	**Minimum Temperature (K)**
No shielding	14 K ± 0.5 K
Aluminium one stage radiation shield (figure 3-2)	8.4 K ± 0.3 K
Radiation shield and superinsulation blanket	5.8 K ± 0.3 K

Table 1. Base temperature achievable upon varying the shielding surrounding the coldhead.

As Table 1 shows, running the pulse tube without any surrounding radiation shielding (with the relevant diagnostics/components attached) meant that the core temperature could not fall below 14 K. Due to the requirement of T<13.9 K to achieve solidification, the system in this state was not suitable for target growth and thus radiation shielding on the first stage was developed. This effectively meant that a 40 K shielding (discounting inherent negative temperature gradient downwards along its surface) surrounded the coldhead, limiting the effects of thermal radiation and dropping the core temperature to a minimum of 8.4 K. Finally, a superinsulation blanket was installed surrounding the radiation shield; increasing the cooling to a minimum temperature of 5.8 K. Thus an 8 K tolerance was achieved between base temperature and the melting point of hydrogen to mitigate the rate of sublimation/target thinning and research into establishing a repeatable growth procedure was commenced.

2.5. Growth Procedure Research:

Upon achieving a suitably low base temperature, work began on establishing a repeatable growth procedure for solidified hydrogen targets in situ. The stability of the temperature sensors between ~6 and 25 K was ± 0.3 K and due to the manual gas injection and readout of the display, pressure readings were accurate to ±20mbar.

As the system is based on the condensation method of hydrogen solidification, referring to Figure 1 it is apparent that the pressure of hydrogen must be above 70.4 mbar in order to pass through the gas:liquid phase boundary.

Once in the liquid regime, the coldhead is further cooled and the vapour pressure maintained by inletting a steady supply of hydrogen into the target chamber due to a pressure decrease resulting from the liquefaction of the gaseous molecules. However, achieving this with this particular setup was difficult as the injection system consisted of a series of manual hand valves and could not be self-regulated. When the temperature of the coldhead passes below ~14 K, nucleation sites within the liquid are observed which initiates the phase transition from liquid:solid and a crystalline solid hydrogen structure then forms as the target freezes.

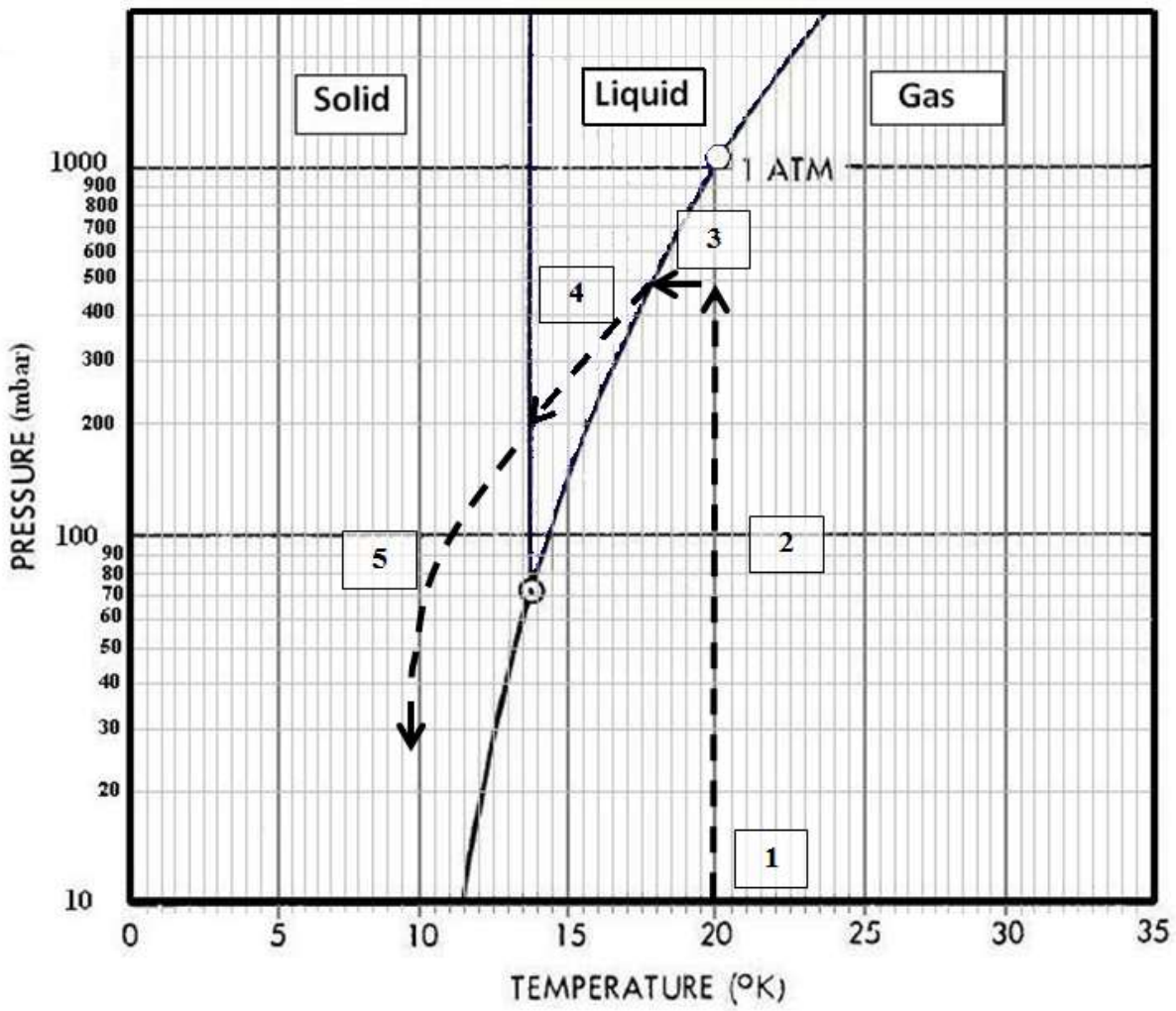

Figure 5. Illustrated phase diagram showing the growth procedure which was devised and followed for in-situ target production.

Referring to Figure 5, there are five relevant stages within the followed growth procedure:

1. The initial state of the system: Regulating the temperature through a temperature controller at 20 ± 0.3 K (above the boiling point of hydrogen).
2. Hydrogen gas injection: The growth chamber is slowly filled with hydrogen until the pressure reaches ~500 ± 20 mbar. This ensures there is a significant pressure to ensure the hydrogen can enter liquid phase as liquefaction causes an inherent pressure decrease.
3. Once there is an appreciable pressure inside the growth chamber, the temperature is dropped and a steady inflow of gas is injected into the chamber to alleviate the pressure drop due to the fall in temperature. When the gas:liquid phase boundary is passed, droplets of hydrogen liquid can be observed flowing down the coldhead/target mount.
4. As liquefaction occurs, there is a sudden pressure decrease within the chamber. Liquid hydrogen begins to flow/drip down the coldhead and over the target aperture: the colder the temperature falls, the lower the vapour pressure and the more viscous the liquid H_2 becomes.
5. When the liquid:solid phase boundary is reached (~14 ± 0.3 K), dependent on the rate of cooling, one or more nucleation sites can be seen on the liquid. From these points, a crystalline structure of solidified hydrogen begins to form, eventually freezing into a thin layer over the target aperture.

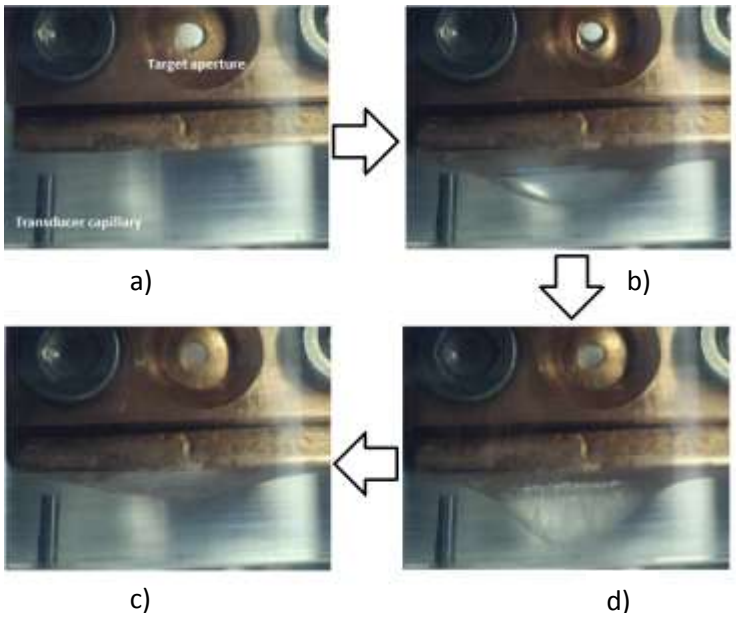

Figure 6. Time-lapse of the growth process. a) Initial state of system at 20 K (stage 1). b) Liquid-phase (stage 4). Note the droplet which subtends from the bottom of the coldhead and the liquid ring over the target aperture. c) Freezing of the liquid film (stage 5). d) Solid H_2 slowly sublimes due to low vacuum conditions within growth chamber. (Images taken with a USB-powered microscope).

The main difficulties realized with this particular system design were:

- *Liquid saturation over the target aperture*: The embedded nature of the target foil – which was sandwiched within the target mount – meant that 'catching' the liquid over the target centre was temperamental and often would take multiple attempts. This was to be revised along with several other design modifications.
- *Fixed/bolted growth chamber*: As the initial configuration was designed as a proof-of-concept, the growth chamber was fixed in place. The ultimate focus of the project was to research the laser interaction with the hydrogen target and as such it is essential that the growth chamber be removable in-situ by designing a removable sealing mechanism.
- *Inaccuracies and non-repeatability of gas injection:* As discussed, the manual nature of the gas injection mechanism led to the fact that maintaining a specific pressure within the growth chamber was difficult. The fluctuations in pressure due to the high sampling rate of the transducer lead to an appreciable error in pressure readout from the display. This could be alleviated by installing data logging hardware/software.

3. Design Modifications

3.1. Dynamic sealing mechanism:

In order to address the experimental issues with the initial system design, several design modifications were made. The primary concern was to design and implement a dynamic sealing mechanism to remove the growth chamber from the coldhead, expose the target to the laser, and reseal the growth chamber, all operated remotely within the control room of the laser facility.

Initial research began on a sealing mechanism which was compatible within the laser chamber i.e. operable at cryogenic temperatures and would enable removal of the the growth chamber from the

proximity of the laser before interaction and would not introduce compressed gases/gas lines nearby. An O-ring seal and a gate valve were not suitable for the application for these respective reasons.

After researching various sealing designs, it was deemed necessary that a motor-drive system would be ideal for the experiment allowing growth chamber withdrawal and re-seal by driving the motor downwards and upwards, respectively. This required that the growth chamber be forced against some sealant material that is reusable and suitable to withstanding the large pressure gradient between the inside of the growth chamber (~100 mbar) and the outer vacuum chamber (10^{-5} mbar).

3.1.1. Sealant material:

The design focussed on placing the sealant material either on the cold head or the rim of the growth chamber and the motor forcing the growth chamber against the coldhead with the sealant material in-between. It was essential that this material should be easily replaceable and adequate for multiple sealings.

Indium pads have been used for similar applications in the past; however this was impractical for this particular setup for two reasons. Firstly, the indium pads are difficult to remove due to the moulding of the metal around the coldhead. Secondly, and importantly, the frequency of reseals would mean regular replacements which are both expensive and time-consuming, which is not ideal during the laser experimental beam-time.

To address the above issues, a novel sealing mechanism, as shown in figure 7, was designed and tested for efficacy. Two and three-bladed knife-edge adapters were machined, to be attached to the rim of the growth chamber which would be forced into a polyimide (Kapton) film of sufficient thickness. The motor drive was initially replicated by a mechanism whereby a threaded screw was centrally aligned on the underside of the growth chamber and set at various torques and forced upwards into a ring of Kapton. This mechanism was then connected to a helium mass spectrometer monitor whereby the area inside the growth chamber is pumped and evacuated and helium gas is injected around the seal. Any helium particles that penetrate the seal are detected by the spectrometer giving a leak-rate; the acceptable value of which for a gas tight seal is < $1x10^{-7}$ mbar·l/sec.[22]

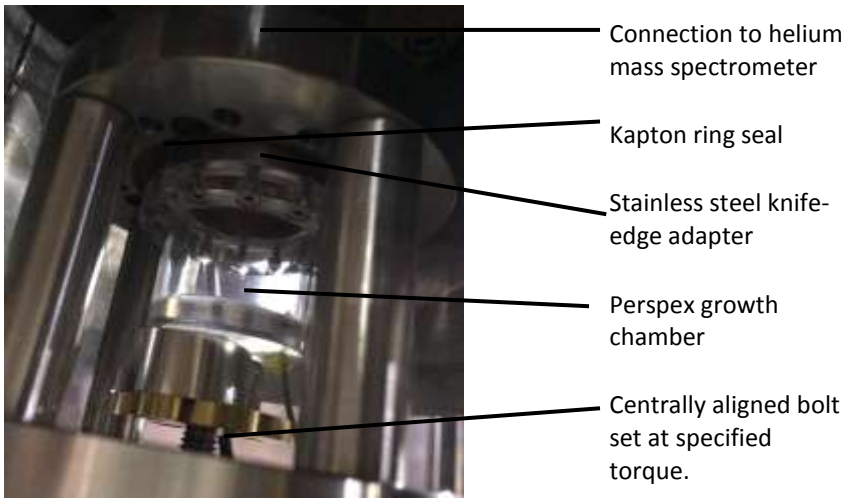

Figure 7. Knife-edge and Kapton sealing leak-rate testing mechanism.

By adjusting the torque on the bolt on the underside of the growth chamber, the force acting upon the Kapton from the knife-edges could be varied; too little torque and the blades did not exert enough force on to the disc to provide a gas-tight seal and too much torque resulted in the blades penetrating the rear of the Kapton again, breaking the seal. The results of the leak testing with two different thicknesses of Kapton with a two-blade and three-blade adapter are shown in figure 8:

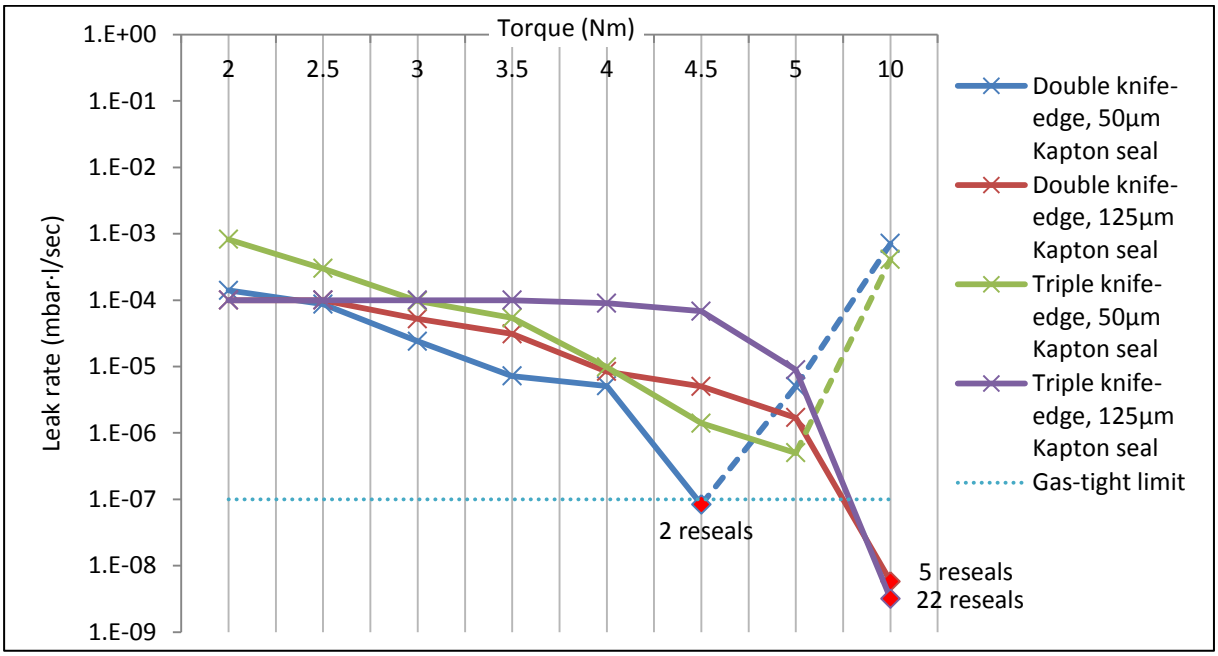

Figure 8. Line graph depicting the leak rates of both a double-edged and triple-edged knife adapter upon different thicknesses of Kapton film (50 µm and 125 µm) when various torques were applied to a bolt forcing the knife-edges into the film. For successful gas-tight seals, the number of repeatable seals are shown.

From the results shown in figure 8, there were only 3 gas-tight configurations of the system. Of the three successful tests, a triple-knife edge adapter under 10Nm of torque forced upon 125 µm of Kapton provided the most leak tight seal of 3.2×10^{-9} mbar·l/sec and was repeatable 22 times at room temperature before the Kapton film failed and needed replacing. Such a result was adequate for use within the laser chamber, meaning that one film installation could last multiple shots. 50 µm films provided better leak rates than the 125 µm films at the same given torque as they were found to be more yielding. However, as illustrated by the dashed lines on the graph, at higher torques the films were cut through completely, leading to a rapid deterioration in the leak rate. For this reason, it was decided that a triple knife-edge adapter against a 125 µm film with a driving torque of 10 Nm would be used for the dynamic sealing mechanism.

3.1.2. Motor drive:

After having established the relevant parameters for achieving and maintaining a gas-tight seal, a remotely controlled motor mechanism was required to allow for the removal/closing of the growth chamber within the laser chamber. This had to be designed to deliver 10 Nm of torque, as well as being sufficiently insulated to avoid undesirable heat loading to the coldhead.

The resulting design was a stepper motor to which the growth chamber was fastened, enabling translational motion and delivering appreciable force onto the Kapton to achieve a gas-tight seal and withdrawal of the mechanism to allow laser access to the hydrogen target after growth, operated from a remote control logic box.

3.1.3. Growth chamber redesign:

Due to the focal length of the optical diagnostics required for monitoring the target, regarding which the author refers to the work of Schaumann G[23], there was a requirement to design a narrower growth chamber. Ultimately, this design resulted in a change in shape of the growth chamber – from a circular to a rectangular footprint which in turn necessitated narrower wall thickness. The knife-edge adapter was also redesigned to match the dimensions of the new design and rather than attached to the rim of the growth chamber due to size constraints was instead bolted onto the base of the coldhead.

After having machined a narrow chamber, integrity testing with the motor revealed cracking in the structure of the perspex material and it was deemed necessary that the walls of the growth chamber required a tougher material which would not be susceptible to fracturing which still allowed visibility of the target. Further testing warranted another redesign which led to the final design of the growth chamber being constructed from stainless steel walls with two quartz optical windows in line with target centre to allow in-situ target viewing. The entire driving mechanism was connected to the coldhead with thermally insulating glass fibre rods.

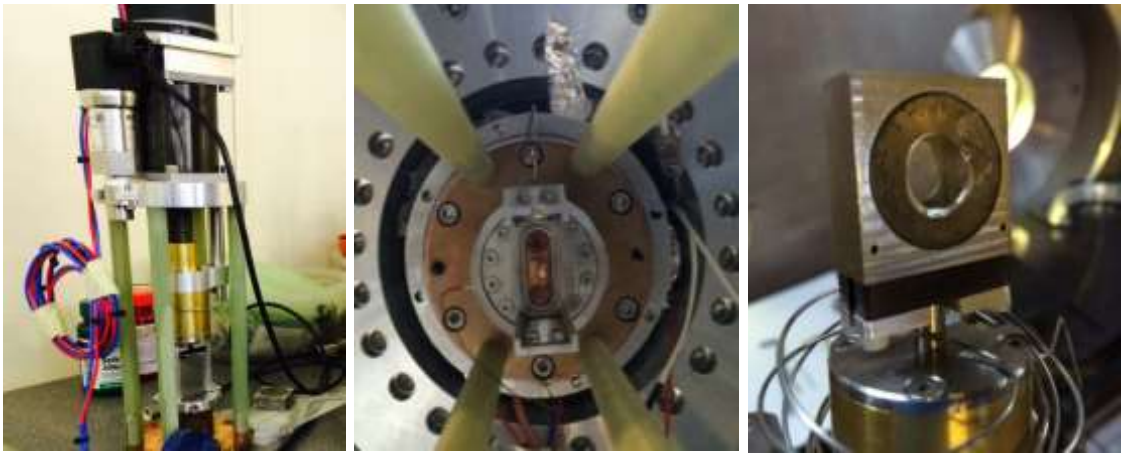

Figure 9: (Left to right) a) 10Nm motor driving mechanism b) Underside view of the mounting brackets for the motor along with the knife-edges. c) Stainless steel growth chamber with transducer capillary.

It is worth noting, however, that due to the large thermal mass in the form of the motor system attached to the base of the coldhead the baseline temperature achievable by the system rose to 9.8 ± 0.3 K with the growth chamber driven into the Kapton and 8.5 ± 0.2 K when the growth chamber was retracted (with superinsulation wrapping in both instances). The change of the material of the growth chamber from an insulating perspex to a conductive stainless steel also added to this rise in temperature. Despite this, the base temperature was still well within tolerance to establish freezing of the liquid hydrogen.

3.2. Gas flow system upgrade:

An automated gas-flow system was commissioned which facilitated the control of the gas pressure inside the growth chamber by using a series of reservoirs and mass flow controllers. This allowed regulation of the flow of hydrogen into and the pumping rate out of the growth chamber in order to maintain a set-point pressure which is crucial in the growth process. This comprised a compact Reconfigurable Input/Output (cRIO) controller which ran through a LabVIEW VI to regulate all aspects of the growth process from a single interface.

The LabVIEW program was modified by Alex Ortner, *Technische Universität Darmstadt*, to incorporate the features necessary for the eventual installation of the experiment into the laser target chamber which included: gas injection/pumping, motor driving, temperature control, data logging and camera viewing. This also meant that human errors were negated from the readout of temperature/pressure values which often fluctuated due to the nature of the system allowing for a more accurate and repeatable growth process.

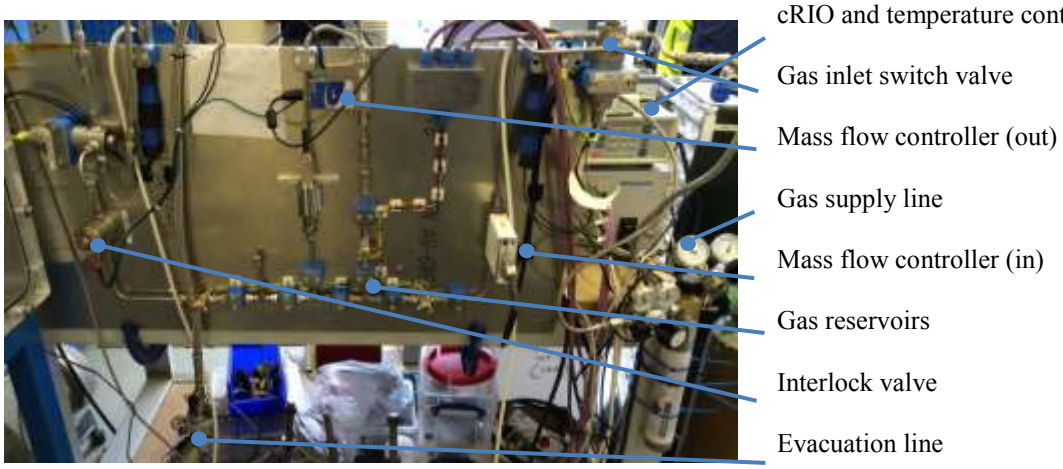

Figure 10: Automated gas-flow system allowing for gas pressure regulation of the growth chamber.

3.3. Temperature control and heater upgrades:

Alongside the integration of the automated gas-flow system an upgrade was necessary to the temperature controller which could only read two temperature sensors simultaneously and output just 27 W of heater power. A model upgrade to the Lakeshore 336 system allowed the monitoring of 4 concurrent sensors and provided 150 W of heater power output. This also allowed for improved PID feedback which improved the temperature regulation of the heaters.

Alternatives were researched in order to improve the warm-up time – roughly 90 minutes with the initial setup. A 100 W and 50 W cartridge heaters were decided upon to both utilise the whole power output of the new temperature controller and to offer volumetric heating as opposed to surface heating. This modification improved warm-up time by a factor of 3 which was crucial to ultimately allow for a higher shot rate.

A further modification was made to the temperature sensors. Initially these were platinum surface mounted sensors which were very susceptible to the effects of thermal radiation and were also difficult to replace which would be necessary due to the potential of EMP damage from the laser pulse. Modified PT-100 temperature sensors were designed and calibrated at Technische Universität Darmstadt which allowed for embedded mounting within the coldhead, leading to a more stable temperature readout from ± 0.3 K to ± 0.1 K (along with an improvement in radiation shielding) at $T < 20$ K. The sensors were attached to replaceable cryogenically compatible connectors to allow for fast in-situ replacement of damaged components.

3.4. Target mount redesign:

Whilst researching a repeatable growth cycle method, there was an intermittent issue in that when the hydrogen gas began to condense, the liquid flow would not always form over the aperture in the centre of the target foil and instead would often trail down the edge of the foil and drip onto the base of the warmer growth chamber, evaporating back into gaseous phase and re-condensing in the same region.

By redesigning the target mount, the target foil was mounted vertically (Figure 11) in order to manipulate the liquid flow down the foil and saturating the aperture in a repeatable manner. After evaluating the cause of the issues with the original target mount/foil (Figure 4), it was found that the graining of the foil was vertical, meaning that liquid flow would follow these contours due to the low viscosity of liquid hydrogen. Owing to the nature of laser cut foils, there was a slight raised edge around the central aperture of the foil forcing the liquid flow around the outer edge preventing saturation over the aperture. By having the foils machined such that the graining was horizontal in the

new design, the liquid was allowed to flow more evenly down the width of the foil and consistently saturate the target aperture.

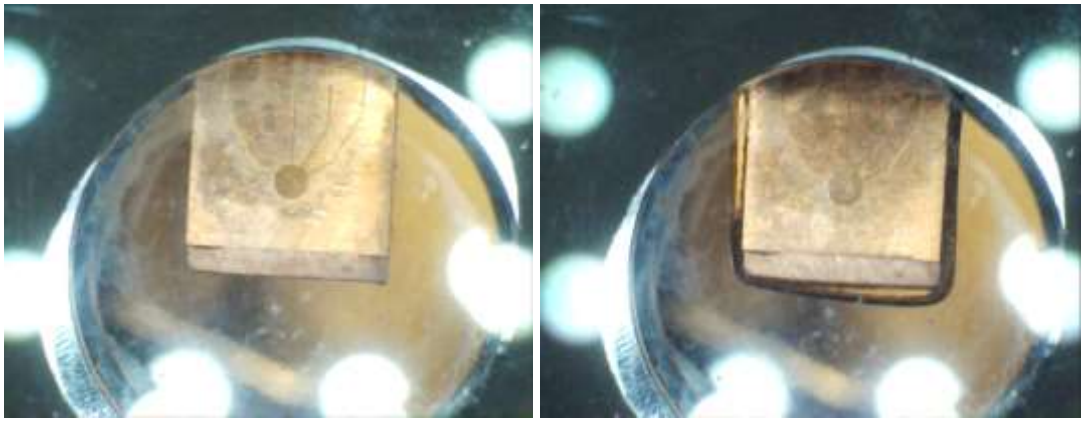

Figure 11: Images of the improved target foils and orientation redesign prior to (left) and after (right) target growth. The foils above have grooves leading towards the centre to promote liquid flow over the target aperture.

3.5. Two-stage radiation shield:

A design adjustment for the existing radiation shield was deemed necessary to further reduce the base temperature of the coldhead. Designing a secondary inner radiation shield connected to the colder (4.2 K) second stage of the pulse tube meant that any radiative heat from the inside of the outer shield would be reflected by the cooler inner shield as opposed to heating the target mount. The design was altered to facilitate the replacement of target foils and temperature sensors by being machined in 2 halves such that the front half could be removed exposing the bolts connecting the target foil to the mount as well as providing access to the temperature sensor connectors.

By integrating the two-stage shield onto the system, a base temperature drop was achieved on the order of ~1.3 K, thereby reducing the minimum temperature achieved by the single stage shield (with superinsulation blanket) from 9.8 ± 0.3 K to 8.5 ± 0.1 K with the growth chamber closed and from 8.5 ± 0.2 K to 7.2 ± 0.2 K with the chamber retracted.

4. Experimental Delivery

In July 2014, the cryogenic targetry system was installed into TAP for an experiment investigating proton acceleration via the BOA mechanism from thin hydrogen targets. By suspending the system from a motorized XYZ stage within a re-entrant chamber on the roof of the target chamber, the position of the target foil could be aligned with the beam axis.

The system was operated in situ, allowing for the first cryogenic target interactions in the Vulcan Petawatt facility since its inception. At the time of writing, data analysis of the results from this experiment is ongoing.

During experimental beamtime it was found that upon retracting the growth chamber to expose the target, the solid hydrogen quickly heated up and sublimed, severely limiting target survival time. Research into this issue led to the conclusion that it was caused by a warm gas effect whereby residual hydrogen ice on the inner edge of (and gaseous hydrogen within) the growth chamber rapidly heated upon losing contact with the coldhead. The escaped gas undergoes heat exchange with the warmer heat loads within the target chamber and is either pumped out or cryo-pumped back onto the coldhead. This latter effect is evidenced by characteristic temperature spikes on the sensors and causes rapid heating of the target. As this is a surface-heating effect, the temperature spike typically lasts for around

30 seconds, rising by approximately 10 K in the original test chamber. This effect had to be accounted for when activating the laser pulse to ensure the target had not sublimed before interaction.

5. Future work and areas of research

As discussed above, an issue of temperature spiking manifested upon retraction of the growth chamber caused by a warm gas effect. There are two methods of assuaging this issue: evacuating the gas to limit the heat loading upon the target from its re-condensation and lowering the achievable base temperature of the target mount to prevent the temperature from rising above the melting point as a result of the temperature spike.

5.1. Mitigation of thermal loading:

To minimise heat loss at the bottom of the target mount due to the temperature gradient stemming from the bottom of the pulse tube, a redesigned target mount adapter is being developed which reduces the length compared to the original adapter (Figure 2).

In order to better understand the heating mechanisms about the target focus has begun on thermal profiling of the system. This required an improvement in the temperature reading accuracy by installing high-precision Cernox™ sensors. Improvements are also being made to the radiation shield and higher quality superinsulation has also been incorporated which will help to further reduce the thermal load.

5.2. Improving pumping capacity:

Experimental observations have shown that the pumping rate is a significant factor in reducing the warm gas effect from heating the target mount; a greater pumping capacity resulting in reduced temperature spiking. Having a larger vacuum chamber volume also alleviates the issue due to greater dispersion of the gas.

A new testing chamber has been built within the CLF to accommodate such modifications which houses two roughing pumps and two turbo pumps with a combined pumping capacity in excess of 2000 l/min, increasing the capacity from the original test chamber by a factor of 4 and improving the vacuum by two orders magnitude.

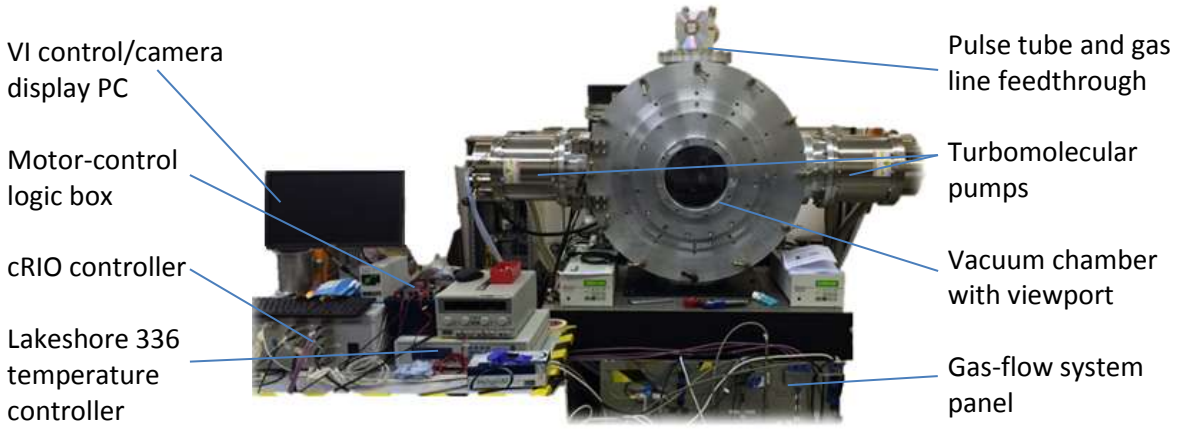

Figure 12: CLF's improved cryo-targetry test chamber.

5.3. Obtaining thinner target films:

After having improved the cooling efficiency and the vacuum of the test system, achieving increasingly thin target films which is preferential in laser-interaction experiments is to be focussed on. Due to issues with diagnostics in measuring and controlling target thickness at the time of writing, the hydrogen films produced by the system are estimated to be comparable to the target foil thickness – on the order of a few hundred microns.

There may be several routes which can successfully achieve this which are intended to be explored, for instance mounting a comparably thin target foil, and target growth via deposition as opposed to the condensation-freezing method, which is possible following the integration of the automated gas-flow system. Reducing the thermal loading upon the coldhead as well as mitigation of the warm-gas effect will be beneficial to this end.

5.4. Target thickness-measurement diagnostics:

In situ thickness measurement has been a key area of research for utilising the system in laser-target interaction experiments and firing upon a target which is too thick will not generate ions of sufficient energy. Due to the volatile nature of hydrogen it is crucial that the thickness of the solid hydrogen film is characterised in real-time to account for the sublimation rate of the target when exposed to the high vacuum and comparatively high thermal loading of the target chamber.

Two methods for target thickness monitoring have been explored: α-source measurement and a confocal chromatic sensor. Obtaining a strong enough signal from the α-source over the working distance within the chamber proved cumbersome and so research in this domain is being focussed on a confocal chromatic sensor system.

5.5. Thermal modelling:

Establishing a clear understanding and simulated model of the thermal effects about the target centre will be crucial to refer to prior to design modifications. COMSOL modelling of the thermodynamic effects due to black-body radiation, convective heating inside the target chamber due to ‘warm’ gas flow upon hydrogen injection and enthalpic contributions due to phase transitioning will be a necessary investigation.

Acknowledgements

The authors gratefully acknowledge funding from EPSRC grant number EP/K022415/1 and in particular to Prof Marco Borghesi for supporting the project.

The authors also gratefully acknowledge funding from Laserlab-Europe grant no. 284464.

CLF would like to extend their gratitude to Gabriel Schaumann, Stefan Bedacht, Alex Ortner (especially for his contribution to the LabVIEW programming), Florian Wagner and Alexandra Tebartz of Technische Universität Darmstadt for their collaboration.

Data associated with research published in this paper can be accessed by contacting the corresponding author.

References

[1] H. Daido et al, Review of laser-driven ion sources and their applications Rep. Prog. Phys. 75, 056401, 2012
[2] Roth M and Schollmeier M 2013 Ion Acceleration: TNSA *Laser-Plasma Interactions and Applications* ed. McKenna P, Neely D, Bingham R and Jaroszynski D chapter 12 pp 329-332
[3] C. Hernandez-Gomez et al, Vulcan petawatt-operation and development, *J. Phys. IV France* **133**, 555-559, 2006
[4] L. Robson et al, Scaling of proton acceleration driven by petawatt-laser-plasma interactions, *Nat. Phys.* **3**, 1, 58-62, 2007
[5] S. C. Wilks et al, Energetic proton generation in ultra-intense laser–solid interactions, *Phys. Plasmas **8***, 542, 2001
[6] J. Green et al, Enhanced proton beam collimation in the ultra-intense short pulse regime, *Plasma Physics and Controlled Fusion*, **56**, 084001, 2014
[7] A. J. Mackinnon et al, Effect of plasma scale length on multi-MeV proton production by intense laser pulses, *Phys. Rev. Lett,* **86**, 9, 1769-1772, 2001
[8] R. Gray at al, Laser pulse propagation and enhanced energy coupling to fast electrons in dense plasma gradients, *New J. Phys*. 16, 113075, 2014
[9] D. Carroll et al, Dynamic control and enhancement of Laser accelerated protons, *Comp. Rendus Physique* **10**, 2-3, 188-196, 2009
[10] D Neely et al, Enhanced proton beams from ultra-thin targets driven by high contrast laser pulses, *Appl. Phys. Lett*. **89**, 2, 2006
[11] C. Brenner et al, Modelling the effect of laser focal spot size on sheath-accelerated protons in intense laser-foil interactions, *Plasma Physics and Controlled Fusion*, 56, 084003, 2014,
[12] Albright B J, Yin L, Bowers K J, Hegelich B M, Flippo K A, Kwan T J T, and Fernández J C 2007 *Phys. Plasmas* **14** 094502-2
[13] M. Borghesi et al, Laser-driven ion acceleration State of the art and emerging mechanisms Nuclear Instruments & methods in physics research A, 740, 6-9, 2014
[14] Yin L, Albright B J, Hegelich B M and Fernández J C *Laser and Particle Beams* **24** pp 291-298, 2006
[15] B. Quai et al, Stable GeV Ion-Beam Acceleration from Thin Foils by Circularly Polarized Laser Pulses, Phys. Rev. Lett 102, 14, 145002, 2009
[16] Roth M, Bedacht S, Busold S, Deppert O, Schaumann G, Wagner F, Tebartz A. and Schollmeier M, Breaking the 70MeV proton energy threshold in laser-proton acceleration and guiding beams to applications. *IPAC2014 conference 15-20 June, 2014*
[17] B. M. Hegelich et al, Laser-driven ion acceleration from relativistically transparent nanotargets, *New Journal of Physics* **15,** 2013
[18] Ishimoto S, Kobayashi T, Morimoto K., Nomura I, Ozawa A, Suzuki S, ... and Tsuru T 2002 *Nuclear Instruments and Methods in Physics Research A* **480** pp 304-314
[19] Markov A N, Fradkov A B and Chemetskii V D 1977 *Sov. J. Quantum Electron.* **7** p 641
[20] Keller C W *et al* 1967 *Handbook of Physical and Thermal Property Data for Hydrogen* p 3.4
[21] Tomlinson S T, Spindloe C, Holligan P and Tolley M 2012 Design for Production of Thin Film Solid Hydrogen Targets *Central Laser Facility Annual Report 2012-2013* p 2
[22] Theoretical Basics and Applications of Helium-Leak Detection 2007 *Pfeiffer Vacuum* http://www.redcross.org.uk/index.asp?id=39992 *Accessed 3 October 2014*
[23] Schaumann G, Bedacht S, Ortner A, Tebartz A, Wagner F, Spindloe C, Astbury S, Hook S, Tolley M and Roth M, Thin Cryogenic Hydrogen Targets for Laser-Driven Ion Acceleration: Fabrication & Characterisation *TFW5 conference 6-11 July 2014*